MYB68 regulates suberin patterning and radially distinct endodermal differentiation

Leonie Kraska[1], Ryohei Thomas Nakano[1a], David Molina[2,3] Laura Ragni[2,3] and Tonni Grube Andersen[1,4]*

Affiliations

1: Department of Plant-Microbe Interactions, Max Planck Institute for Plant Breeding Research. Carl-von-Linne-Weg 10, 50829, Cologne, Germany.

2: ZMBP, Center for Plant Molecular Biology, University of Tübingen, Germany

3:University of Freiburg, Institute of Biology II, Schänzlerstr 1, 79104 Freiburg, Germany

4: Cluster of Excellence on Plant Sciences (CEPLAS), Cologne, Germany

[a] Current address: Department of Biological Sciences Faculty of Science, Hokkaido University

*Corresponding author: tandersen@mpipz.mpg.de

Key words: Endodermis, passage cells, cytokinin, tissue patterning, suberin, root vasculature

Roots are composed of concentric tissue layers that enable selective uptake of nutrients, attributed to the vascular-embracing endodermis. In mature root regions, endodermal cells coat their cell surface in a hydrophobic polymer termed suberin, which blocks solute transport across the plasma membrane. Intriguingly, specific cells adjacent to the water-conducting xylem remain unsuberized. These are termed “passage cells” based on the assumption that they create a “passage” for nutrient influx into vasculature in the otherwise sealed-off root regions. The identity and function of passage cells remain unknown, but their presence proposes the existence of individual identities within the endodermis. In this study, we probe this by performing an in-depth investigation of passage cells and endodermal suberization in the model plant *Arabidopsis thaliana*. Our work identifies the transcription factor MYB68 as a key regulator of suberization and endodermal lineage-specification related to passage cell formation. Through transcriptional profiling of *myb68* mutants, we unravel genes with passage cell-associated expression that suggest a function in cation homeostasis. Collectively, our findings create a framework for a deeper understanding of radial cell identities within the endodermis and highlight that dynamic spatiotemporal patterning is an important physiological feature of root ground tissues.

Introduction

To facilitate efficient nutrient uptake, roots consist of multiple concentric tissues that surround the inner vasculature. This organization is crucial for selective absorption and translocation of solutes between the above- and below-ground plant parts. In *Arabidopsis thaliana* (hereafter Arabidopsis), the outer tissues comprise the soil-facing epidermis and two related layers: the cortex and the endodermis, which combined make up the ground tissues (Dolan, et al., 1993). The underlying vasculature is organized in opposing xylem and phloem poles responsible for water/minerals and photoassimilate transport respectively. Particularly the endodermis provides protection for the vasculature, as it contains barriers that are key for selective nutrient uptake (Geldner, 2013). Across the endodermal circumference, the individual cells are positioned adjacent to the xylem or phloem poles (xylem pole-associated endodermis, XPAE or phloem pole-associated endodermis, PPAE respectively) or in-between these (non-pole-associated endodermis, NPAE). Interestingly, after 1-2 weeks of growth, sporadic formative divisions in the meristematic XPAE initiate an additional ground tissue layer called the middle cortex (MC) (Baum, et al., 2002). The function and genetic program underlying MC cells is not fully understood, but their existence propose that XPAE cells may follow a specialized developmental program that is inferred from xylem-related mechanisms (Baum et al 2002), (Paquette and Benfey, 2005).

As cells exit the meristematic root tip and initiate maturation, the endodermis undergoes two consecutive stages of differentiation before shedding due to secondary growth (Wunderling, et al., 2018; Geldner, 2013). The first involves deposition of the lignin-based apoplastic barrier known as the Casparian strip (CS) in the cell walls between endodermal cells (Caspary, 1865). This feature prevents unspecific diffusion across the endodermis and forces uptake to occur actively across the plasma membrane (Priestley and North, 1922). The second stage is defined by the occurrence of a hydrophobic fatty-acid-containing polymer called suberin. Suberin is deposited as a lamellae-like structure around the entire cell (Franke, et al., 2005; Sitte, 1959). This blocks transport across the plasma membrane, which in combination with the CS, effectively isolates the vasculature from its external surroundings in older root parts (Andersen, et al., 2015).

In 5-6-day-old Arabidopsis seedlings, suberization occurs approximately 15-20 cells after the formation of the Casparian strip (CS) and follows a stereotypical pattern along the longitudinal root axis (Alassimone, et al., 2010). The decision of individual cells to undergo suberization occurs in a non-coherent pattern and is initiated slightly earlier in the PPAE cells than in XPAE (Andersen, et al., 2018), which leads to a "patchy zone" of suberization. This patchy region spans 10-15 cells before establishment of a "fully suberized" zone that covers the remaining portion of the endodermis until the root-hypocotyl junction. In support of a specialized developmental programming, individual cells in the XPAE remain unsuberized throughout the entire development (Holbein, et al., 2021; Andersen, et al., 2018; Peterson and Enstone, 1996; Kroemer). These are referred to as endodermal “passage cells” (PCs), as the circumvention of suberin deposition has historically been thought to provide a low-resistance flow directly into the xylem (Peterson and Enstone, 1996; Kroemer). Although PCs were identified over a century ago and have been observed in many plant lineages (Holbein, et al., 2021), genetic insights into their function and development have only recently begun to emerge. In Arabidopsis, PCs are initiated in the meristematic XPAE by radially coordinated hormonal signaling in the vasculature (Andersen, et al., 2018). The exact genetic program(s) that underlie this is still not understood, but establishment of the PC identity depends partially on radial diffusion of the cytokinin signaling repressor ARABIDOPSIS HISTIDINE PHOSPHOTRANSFERASE 6 (AHP6) (Andersen, et al., 2018; Mähönen, et al., 2006). Intriguingly, although MC cells are also initiated in this region, it is currently unknown if these are connected to PC establishment. Several transcription factors (TFs) belonging to the R2R3-MYB (myeloblastosis) class play essential roles in endodermal differentiation (Shukla, et al., 2021; Kamiya, et al., 2015; Liberman, et al., 2015), suggesting this class of TFs may harbour other factors that influence endodermal patterning.

In this study, we set out to investigate the formation of PCs in detail and to identify factors that control their establishment. Through a high-resolution spatiotemporal analysis of the suberization process in a number of mutants, our work identifies the CS-master regulator homologue MYB68 as an important factor in the establishment of endodermal identities. We find evidence that MYB68 is a negative regulator of both PC and MC formation and control distinct gene expression in both cell-types. Moreover, our findings highlight the existence of an age-dependent dynamic regulation of the suberization process, which is linked to PC establishment and MC formation.

Combined, this emphasizes the existence of mechanisms that determine radial endodermal maturation and provides an updated framework for ground tissue differentiation that includes spatiotemporal dynamics.

Results

MYB68 is a regulator of endodermal suberin patterning

To start our investigation, we focused on a subclade of R2-R3 MYB domain-containing TFs, which includes the master regulator of CS formation MYB36 (Kamiya, et al., 2015; Liberman, et al., 2015). We hypothesized that within this clade, other members may play roles associated with endodermal differentiation. This subfamily comprises six members: MYB36, MYB37, MYB38, MYB68, MYB84, and MYB87, for which we recently established homozygous knockout mutant lines (Molina, et al., 2024). To assess whether these were affected in endodermal development, we examined the functionality of the CS and measured suberin patterning in 6-day-old roots. Consistent with previous findings (Molina, et al., 2024; Kamiya, et al., 2015), *myb36-2* exhibited a dysfunctional apoplastic barrier, evidenced by a significantly increased propidium iodide (PI) penetration (Naseer, et al., 2012), while all other tested mutant alleles resembled wildtype (Col-0) (**Figure 1A, Figure S1A**). Regarding suberization, *myb36-2* displayed an early onset directly associated with its impaired CS function (Doblas, et al., 2017). *myb68* alleles exhibited a significantly increased patchy suberization zone albeit, the lack of suberization appeared to be restricted to distinct cell files (**Figure 1B,D**,**Figure S1B**). To investigate whether this was related to a general defect in the ability to synthesize or deposit suberin, we exposed *myb68* roots to 1 uM ABA for 2 days (Barberon, et al., 2016). This resulted in a significant increase in suberization in both Col-0 and *myb68* roots (**Figure 1C** and **Figure S1B**), demonstrating that *myb68* roots are capable of endodermal suberin deposition. Thus, we conclude that within the subclade of MYB TF investigated, MYB68 functions in a genetic network related to endodermal suberin patterning.

MYB68 represses endodermal passage cell occurrence

To further examine the apparent cell-file-specific suberin-related changes observed in *myb68* roots, we meticulously quantified radial suberization along the root. Intriguingly, when compared to Col-0, 6-day-old *myb68-2-4* roots displayed a delay in the onset of suberization in all endodermal cells (**Figure 2A**). However, in the PPAE, this difference

in pole-specific suberization was only significant in the youngest of the analyzed root part (just after the patchy zone) whereas XPAE and NPAE cells had an almost complete absence of suberization across the entire measured region (**Figure 2A**). Hence, MYB68 influences the general decision for the onset of suberization, but plays an important role in establishing suberin deposition in non-PPAE cells. One additional noteworthy finding in this analysis was that in Col-0, we identified a restricted area of endodermal cells near the hypocotyl, which was unsuberized (**Figure S1C**).

To probe if the changed suberin pattern in *myb68* roots is related to PCs, we introduced a transcriptional marker for the PC-expressed *phosphate exporter homologue* 3 gene (*PHO1;H3*) (Andersen, et al., 2018) into Col-0 and *myb68-2-4* backgrounds. We then quantified the amount and position of endodermal cells with *PHO1;H3* activity across multiple lines. As previously observed, in Col-0, this marker displayed a bias of *PHO1;H3* activity towards XPAE and NPAE cells (**Figure 2B**). However, in roots with *myb68-2-4* background, this pattern was exaggerated as significantly more XPAE and NPAE cells exhibited expression when compared to the Col-0 background lines (**Figure 2B, Figure S1D**). Although PPAE cells also showed a significant increase in *PHO1;H3* activity (**Figure 2B, Figure S1D**), the strong bias towards non-PPAE cells corroborates the suberin pattern found in this mutant and thereby indicates that MYB68 function is linked to PC occurrence. In further support of this, germination of *myb68-2-4* plants on increasing concentrations of the artificial cytokinin benzylaminopurine (BAP) led to a dose-dependent expansion of the fully suberized zone in *myb68-2-4* roots (**Figure 2C**). As germination on low amounts of BAP has previously been observed to repress PC formation (Andersen, et al., 2018), this is in line with repression of an exaggerated PC occurrence in *myb68.*

Assymetric expression of *MYB68* in the meristem proposes a role in radial endodermal identity establishment.

To dissect whether the observed effects of MYB68 were locally influencing PCs or related to their initiation in the meristematic region, we next investigated its expression pattern. To accomplish this, we constructed fluorescent transcriptional reporter lines that used the entire intergenic region between *MYB68* and its upstream gene to drive the expression of a nuclear-localized fusion reporter (NLS 3xmVenus). By analysing multiple lines of 6-day-old roots carrying this construct, we found promoter activity in endodermal cells corresponding to the suberization zone, while other tissues such as

the stele also showed activity (**Figure 3A**). This is in line with MYB68 also playing a role in the stele-derived periderm (Molina, et al., 2024) and corroborates a role in the endodermis tied to suberization. Indeed, when expressed under the non-meristematic endodermis-specific promoter ELTP, which is active right after formation of the CS (Barberon, et al., 2016), ectopic presence of MYB68 repressed the occurrence of pre-established PCs as well as decreased the patchy zone with only a minor effect on the onset of suberin deposition (**Figure S2A, S2B**). The *MYB68* promoter also exhibited activity in the meristematic region (**Figure 3A**), which is not the case for known suberin-inducing MYB transcription factors (Shukla, et al., 2021; Kosma, et al., 2014). Here, PPAE lineages showed expression immediately after the cortex endodermis initial daughter cell (CEID), while XPAE and NPAE lineages had a significantly later onset of expression towards the distal meristem (**Figure 3B, Figure S2C,D**).This difference in expression onset in the endodermis could be dose-dependently by germination on similar levels of BAP that affected the suberization pattern (**Figure 3C, Figure S2E).** Taken together, this suggests that besides a likely role in controlling the decision to suberize locally in the individual cells, MYB68 may also be involved in patterning events in the meristematic region.

MYB68 regulates age-dependent pre-patterning of endodermal differentiation

One additional observation in our expression analysis was that the radial asymmetric endodermal onset of *MYB68* expression shifted from its close proximity to the CEID towards more distal cells over time (**Figure 3D, 3E, Figure S2F,G**). This proposes the existence of an age-dependent mechanism influencing the suberization pattern. To test this, we conducted a time-course analysis in 3-11-day-old roots. This window encompasses the young embryonic endodermis before onset of suberization, until periderm formation (Serra, et al., 2022; Wunderling, et al., 2018). In Col-0 roots, we observed the fully suberized zone to become longer over time (**Figure 3F**). This was anticipated, since the decision to suberize must correlate with root age and the forming periderm is also suberized (Wunderling, et al., 2018). Unexpectedly, the region of the root displaying patchy and unsuberized zones also correlated positively with increased root length (**Figure 3G**). Thus, the decision of the individual endodermal cell to undergo suberization appears to be delayed as the root ages. This appears to be exaggerated in *myb68-2-4* as the patchy zone increased faster and the fully suberized zone slower compared to Col-0 (Figure 3G Table S2). Additionally, linear correlation analysis of suberization in the patchy zone showed that in *myb68-2-4* this patterning had different

dynamics than Col-0, as we found an increased residual standard error in the fitted model when compared between the two genotypes, revealing *myb68-2-4* suberization pattern to be not constant over time (**Figure S2H, Table S2**).Thus, we conclude that MYB68 influences an age-dependent suberin patterning of the endodermis by regulating the decision to suberize or form PCs.

MYB68 interplays with AHP6 in regulating passage- and middle cortex cells

To investigate how MYB68 ties into the known network underlying PC establishment, we crossed our *myb68-2-4* allele to the *ahp6-1* mutant, which displays reduced PC occurrence when compared to Col-0 (Andersen, et al., 2018). In this analysis, *ahp6-1* roots exibited an increase in suberization of XPAE and NPAE cells (**Figure 4A**). However, under our growth conditions, this was only different from Col-0 in the early parts of the suberization zone. Both the *myb68-2-4* and the double knockout *(*dko) displayed a strong reduction of suberization across all cell files in the early suberization zone (around 60% distance from the root tip), whereas in the later parts, this was specific to XPAE and NPAE cells (**Figure 4A**). Thus, with regards to suberization, MYB68 appears to be epistatic or independent of AHP6. Another characteristic of the XPAE cells is that they are shorter than those in the PPAE, and this difference depends partially on AHP6 (Andersen, et al., 2018) (**Figure 4B**). In our measurements, *myb68-2-4* plants displayed the opposite behavior, as these roots had a significantly decreased length of XPAE cells, which was reverted back to Col-0 levels in the dko (**Figure 4B).** Thus, MYB68 and AHP6 enforce contrasting effects on the XPAE cell lengths. One additional distinctive feature of the XPAE is the initiation of MC cells (Paquette and Benfey, 2005; Baum, et al., 2002). To analyse if MC occurrence was affected in the tested mutants, we grew plants on mesh-containing plates as this gave a consistent establishment of MC under our growth conditions. Also here, when compared to Col-0, *myb68-2-4* and *ahp6-1* single mutants displayed a significantly in- and decreased occurrence of MC cells respectively, which was reduced to Col-0 levels in the dko (**Figure 4C**)*.* Thus, similar to their effect on cell length, MYB68 and AHP6 impose opposite effects on the periclinal division leading to MC cells. Taken together, these findings support a model where MYB68 serves in a network with AHP6 to repress PC and MC formation through control of cell division, but play an independent role in regulating suberization.

A subset of potassium transport-related genes are expressed in passage cells

Next, we set out to use the increased PC occurrence in the *myb68-2-4* mutant to probe the transcriptional identity of PCs. Based on our analysis, we reasoned that genes associated with PCs would have to fulfill two criteria: 1) increased expression in *myb68-2-4* when compared to Col-0 *2)* show similar expression levels in *myb68-2-4* as Col-0 when treated with BAP. To accomplish this, we analysed the root transcriptome of 6-day-old WT and *myb68-2-4* plants germinated in the presence of mock or 25 nM BAP, as this completely reverted the suberin pattern of *myb68-2-4* to that of Col-0 (**Figure 2C**)**.** We then compared the upregulated DEGs between mock-treated *myb68-2-4* and Col-0 roots ($P_{adj.}$ <0.05) to the non-DEGs in a comparison between these genotypes treated with BAP. 66 genes fulfilled both criteria (**Figure 5A, Table S4**) and a gene ontology (GO) analysis (Zhou, et al., 2019) of this subset showed significant enrichment in functions such as “inorganic cation transmembrane transport,” “response to gibberellin” and “regulation of cell communication and signaling” (**Figure 5B**). These functions are in line with previously proposed roles of PCs in nutrient homeostasis as well as biotic communication (Holbein, et al., 2021). Moreover, as MCs have been shown to be controlled, amongst other factors, by gibberellic acid (GA), the increase of MCs in *myb68-2-4* corroborates that this particular GO term was enriched. Indeed, several MC-connected genes were differentially expressed in *myb68-2-4,* including *SCARECROW LIKE 3* (SCL3) *SCL3* and RGA-LIKE PROTEIN 3 (*RGL3) (Yoshida, et al., 2014; Zhang, et al., 2011)* (**Figure 5C**).

We then shifted our focus to investigate the transport-related GO term in more detail. Within this, we identified two potassium (K) transporters *POTASSIUM UPTAKE 8* (*KUP8) and HIGH AFFINITY K+ TRANSPORTER 5 (HAK5)* (Osakabe, et al., 2013; Gierth, et al., 2005) as well as the Arabidopsis sodium (Na) transporter *HIGH-AFFINITY K+ TRANSPORTER* 1 (*HKT1)(Mäser, et al., 2002)* (**Figure 5C, Table S6***)*. To probe if these genes are associated with PCs, we created promoter-based transcriptional marker lines or performed whole-mount hybridization chain reaction fluorescent *in situ* hybridization (HCR-FISH) (Oliva, et al., 2022). Interestingly, in the suberizing part of 6-day-old roots, both *KUP8* and *HAK5* showed expression in the endodermis, which was biased toward XPAE or NPAE cells and increased in the *myb68-2-4* line (**Figure 5D**). *KUP8* showed activity in both endodermis and the pericycle, whereas *HAK5* mRNA was, besides the endodermis, also localized in cortex and epidermal cells **(Figure 5D)**. In contrast to these genes, *HKT1* displayed no obvious pole-associated bias within endodermal cells of any type, yet its endodermal

expression was significantly increased in *myb68-2-4* **(Figure 5D, Figure S3)**. Notably, all three genes also showed expression in an additional cortex layer close to the hypocotyl, which appeared similar to MC cells (Scheres, et al., 1994) (**Figure 5D)**. Combined these observations identify novel PC-associated genes and proposes that PC (or at least non-PPAE cells) as well as MC cells play an unknown role in K/Na homeostasis.

Discussion

In this work, we propose a dual role of MYB68 as a regulator of radial suberin patterning and cell lineage specification within the root endodermis. MYB68 was recently found to activate suberin-related promoters via an *in-planta* assay (Molina, et al., 2024) and enable suberization in rusetting of apples (Xu, et al., 2023). Thus, it likely plays a role in controlling expression of genes involved in production of suberin and thereby influences the suberization within the individual endodermal cells. However, similar to recent observations done on MYB68 function in the periderm (Molina, et al., 2024), our analyses propose that MYB68 serves at least one additional function.

As we found MYB68 to regulate suberization in endodermal cell files that can establish PCs and be expressed in the meristem, we argue that this is related to a previously proposed model for PC establishment (Andersen, et al., 2018). The foundation of this model is that the threshold for onset of suberization within the individual endodermal cell depends on its spatial association with the underlying prevascular cells. Through radially distinct auxin and cytokinin distribution in the procambium and vasculature layers (De Rybel, et al., 2016) low and high cytokinin signaling is established in XPAE and PPAE cell files, respectively. This affects the sensitivity of the individual endodermal cell for suberin-inducing signals, which accumulate as the cell matures until the threshold is passed and the decision to suberize is made (**Figure 6A**). The outcome of this is that PPAE cells can maintain a robust path towards suberization while XPAE cells are faced with the possibility to initiate a developmental direction that leads to PC establishment rather than suberization (**Figure 6A**) (Andersen, et al., 2018). Our analyses support a role for MYB68 in this model as a signal that modulates the likelihood for suberization within the endodermal cell files rather than affecting the hormonal sensitivity (**Figure 6A**). Thus, early *MYB68* expression in the PPAE could be a mechanism providing robustness to the suberization decision within these cells, while its absence in the young XPAE allows these cells to select a trajectory that either leads

towards suberization or PC identity. However, since the suberization pattern as well as *PHO1:H3* expression in *myb68* roots was least affected in PPAE and NPAE cells, additional MYB68-independent mechanisms must exists which positively affects suberization decision in the PPAE. This is supported by a recent study which, via a modeling approach, proposed a role for GA in PPAE suberization (Binenbaum, et al., 2023). Moreover, our analyses expands on this model by proposing that the hormonal sensitivity of the XPAE cells is not solely determined by AHP6, but likely also other unknown cytokinin-responseive factors present in the XPAE (**Figure 6A**).

Intriguingly, since the shorter length of XPAE cells has been found to be due to increased cell division (Andersen, et al., 2018), MYB68 likely additionally functions in a mechanism that represses both peri- and anticlinal divisions in the meristematic XPAE. This is in agreement with a recent analysis identifying MYB68 as a repressor of cell divisions in the periderm (Molina, et al., 2024). MC cells normally occur in older roots, which coincides with a spatial delay in MYB68 expression as well as an appearent MYB68-dependent change in the suberization pattern (**Figure 3F**). Taken together, we therefore propose that, besides functioning as part of a spatially coordinated regulatory network that informs endodermal cell differentiation, MYB68 also plays a role in an age-regulated mechanism that integrates XPAE divisions (both PC and MC cells) with suberization patterns in the mature root parts (**Figure 6B**).

Despite their existence across most plant lineages, very little is known about the function of PCs. Based on gene expression patterns, they likely serve a role in nutrient-related transport processes (Holbein, et al., 2021; Lin, et al., 2009; Hamburger, et al., 2002; Gaymard, et al., 1998). In line with this, our work identifies the genes coding for the high-affinity K-transporters HAK5 and KUP8 as PC-associated and thereby proposes a role in K-homeostasis. Interestingly, we did not pick up previously established PC genes in our analysis such as *PHO1* or its homologes (Andersen, et al., 2018; Hamburger, et al., 2002). Thus, our criteria for PC-association may have created an increased occurrence of false negatives for PC-associated gene expression and thereby limited the resolution of our analysis.

HKT1 has been consistently reported show specific expression in the stele (DAVENPORT, et al., 2007; Sunarpi, et al., 2005; Berthomieu, et al., 2003; Mäser, et al., 2002), and play an important role in retrieval of Na from the xylem sap before transport to the shoot (DAVENPORT, et al., 2007). However, these studies employed

a relative short promoter region to drive *HKT1* expression. Thus, the difference in our expression pattern may lie in the inclusion of the entire intergenic region. Indeed, the intergenic region upstream of *HKT1* includes additional regulatory elements that affect *HKT1* expression (Baek, et al., 2010) and function (Nawaz, et al., 2019). Thus, the truncated promoter region in these studies are likely insufficient to fully explain the role of HKT1 in other areas of besides the stele. Intriguingly, *HKT1*, *KUP8* and *HAK5* were all expressed in a small junction-zone between root and hypocotyl, which also included less suberin and increased PC/cortex formation (**Figures 5D and S1C**). We speculate that this zone may serve to store toxic ions in ground tissue cells, as cortex proliferation has been suggested to be beneficial in abiotic stress conditions (Cui, 2015; Cui, et al., 2014) . One intriguing aspect of this idea is that these cells are shed off during secondary growth and periderm formation. Thus, loading of toxic or excess ions into this zone would allow a fascinating ability to expel toxic ions by loading them into cells destined be explused. As PCs occur across most plant lineages, this may have important implications for our understanding of root functions in cation homeostasis and abiotic stress tolerance.

Figure legends

Figure 1 Formation of endodermal barriers in MYB36-clade mutants A) Quantification of Casparian strip function by measuring the absolute distance from the root tip to the onset of PI penetration blockage into the vasculature (Naseer, et al., 2012). B), C) Suberization patterning in roots stained with the dye Fluorol yellow 088 (FY) (Naseer, et al., 2012). D) Images depict part of the suberized zone of FY (LUX, et al., 2005) roots. Individual letters depict significance (P<0.05) according to a Kruskal Wallis test with a *post hoc* Nemenyi test. Scale bar represents 100 µm. In A, asterisks depict significant difference to WT according to unpaired Wilcoxon test, whereas in D, asterisks mark individual passage cells. ABA; Abscic acid

Figure 2 Analysis of suberin patterning and passage cell occurence

A) Analysis of radial suberin patterning along the upper 50% of the root. Roots were fixed and stained with Fluorol Yellow 088 (FY) (LUX, et al., 2005) and the proportion of suberized cells were quantified and binned in longitudinal sections. Asterisks indicate significant difference between Col-0 and *myb68-2-4* in each longitudinal position according to students Welch two sample t test (* p value < 0.05, ** p value < 0.005, *** p < 0.0005). B) Proportion of endodermal cells with expression of *PHO1H3*

in XPAE vs PPAE of the upper 50% of the root (similar sections as in A). Stars indicate significant difference between WT and *myb68-2-4* in each longitudinal position according to unpaired Wilcoxon test (* p value < 0.05). C) Suberization pattern in roots grown in presence of increasing amounts of the artificial cytokinin 6 Benzyl-aminopurine (BAP). Individual letters depict significance (P<0.05) according to a Kruskal Wallis test with a *post hoc* Nemenyi test. XPAE; Xylem pole associated endodermis, PPAE; Phloem pole associated endodermis, NPAE; Non-pole associated endodermis.

Figure 3 Analysis of *MYB68* expression and age-dependent suberin patterning

A) Activity of *MYB68* in roots of 6-day-old seedlings expressing a transcriptional reporter for *MYB68* activity (*pMYB68*:NLS3xVenus). Roots were fixed in Clearsee and cell walls were stained using calcofluor white (Ursache, et al., 2018) Scale bar represents 50 µm. The two dashed lines mark the position of cross sections I and II. B) Analysis of expression onset of *MYB68* in the meristematic zone of plants from A. Individual letters show significance according to Kruskal Wallis test with *post hoc* Nemenyi test. C) Changes of *MYB68* expression onset in roots germinated in the presence of increasing amounts of the artificial cytokinin 6 Benzyl-aminopurine (BAP). Onset is normalized to the average of nontreated roots in each radial position. Asterisks indicate significant differences compared to the untreated sample in each radial position according to unpaired Wilcoxon text (* p value < 0.05, ** p < 0.001, *** p < 0.0001). D) Expression onset in the endodermis of *MYB68* measured along a time course (Linear regression statistics can be found in Table S1). E) Images depicting *MYB68* expression start within the meristem 5- and 9-day-old roots expressing a MYB68 transcriptional reporter similar as A. Arrows marks the cortex/endodermal initial daughter cell (CEID). Scale bar represents 50 µm. F) Time-course analysis of suberin patterning in 3-11 day-old roots stained with fluorol yellow 088 (LUX, et al., 2005). Asterisks indicate significant differences between Col-0 and *myb68-2-4* at each time point, and in each zone via an unpaired Wilcoxon text (* p value < 0.05, ** p value < 0.005, *** p value < 0.0005). G) Relation of suberization zone length to root length of individual roots in 5-11-day old roots. Values for the slopes are displayed (m). Corresponding statistical values can be found in Table S2. XPAE; Xylem pole associated endodermis, PPAE; Phloem pole associated endodermis, NPAE; non-pole

associated endodermis. Ep; epidermis, co; Cortex, en; Endodermis, st; Stele. XP; Xylem pole, PP; Phloem pole.

Figure 4 Analysis of endodermal cell characteristics

A) Analysis of radial suberin patterning along the upper 50% of the root. Roots were fixed and stained with Fluorol Yellow 088 (FY) (LUX, et al., 2005), and the proportion of suberized cells was quantified and binned in longitudinal sections. Individual letters show significance according to an ANOVA test with a *post hoc* Tukey´s HSD paired T-test. B) Endodermal cell lengths of 6-day-old roots fixed and stained with calcofluor white (Ursache, et al., 2018). Individual letters show significance according to Kruskal Wallis test with post hoc Nemenyi test. C) Measurement of middle cortex (MC) occurence in 6-day-old roots grown under mesh conditions. The graph depicts the distance from the first-occuring MC to the root tip. Asterisks indicate significant difference to WT according to unpaired Wilcoxon text (* $p < 0.05$). XPAE; Xylem pole associated endodermis, PPAE; Phloem pole associated endodermis, NPAE; non-pole associated endodermal cells.

Figure 5 Passage cell-associated transcriptional analysis

A) Overlap of upregulated genes in 6-day-old Col-0 vs *myb68-2-4* roots (p_{adj} <0.05) and genes with non-significant changes in WT vs. *myb68-2-4* when germinated on BAP (25 nM 6-Benzyl-aminopurine). B) GO-term analysis of the 66 overlapping genes from A (Zhou, et al., 2019)C) Heatmap of selected middle cortex (MC) regulating genes as well as cation transporters in the comparisons from A (all genes can be found in **Table S6 and S7**). D) Quantification of transcriptional activity of gene expression in the upper 50 % of the root as well as MC-like cells close to the root-hypocotyl junction. Expression analysis of *KUP8* and HKT1 in WT and *myb68-2-4* was performed using the corresponding transcriptional marker lines (*pKUP8*:NLS3xVenus, *pHKT1*:NLS-3xmScarlet). For *HAK5* mRNA, fluorescence *in situ* hybridization was employed. As negative control either a probe specific for the Bacillus subtilis dapB (LOT # RTB 421) with the corresponding amplifier B1h1 (LOT #S046325) and B1h2 (LOT # S050925) or only the amplifier used for *HAK5* B3h1 (LOT#S073325) and B3h2 (LOT#S075725) without a probe were used. Individual letters show significance according to Kruskal Wallis test with post hoc Nemenyi test. XPAE; Xylem pole associated endodermal cells, PPAE; Phloem pole associated endodermal cells, NPAE; non-pole-associated

endodermal cells. Ep; Epidermis, Co; Cortex, En; Endodermis, nd; not detected, ns; not significant. Scale bars represent 25 µm unless otherwise mentioned.

Figure 6 Model of radial endodermal development

(A) Depending on the radial position in relation to the vasculature, endodermal cells have a different threshold for suberization. In the xylem pole-associated endodermis (XPAE), the presence of the cytokinin signaling repressor AHP6, as well as other unknown factors, increases the threshold, whereas the absence of these in the phloem pole-associated endodermis (PPAE) lowers the threshold. In this model, MYB68 influences individual cells to have a higher or lower probability to be suberized. Because of the low threshold in PPAE, progression of cells through development results in increasing suberin inducing signals in all cells, which renders PC formation to only be possible in XPAE. (B) With aging, *MYB68* expression moves up to the basal meristematic region. This correlates with later suberization in older roots. Additionally, since MYB68 repress cell divisions, this shift in expression allow middle cortex (MC) formation/ periclinal cell division to occur in older roots. MYB68 leaves the apical meristem from day 6/7. Subsequently, MC formation starts.

Figure S1 Endodermal barriers (A) Quantification of Casparian strip integrity by measuring the distance from the root tip to the onset of PI penetration as described before (Naseer, et al., 2012). Star indicated a significant difference to WT according to the unpaired Wilcoxon test. (B) Staining of suberin using the dye Fluorol yellow (FY) (Naseer, et al., 2012), graphs depict the relative proportion of the root which is unsuberized (white), suberized in a patchy pattern (grey), and fully suberized (yellow). Transfer to 1µM ABA or mock 2 days before staining. Individual letters show significance according to the Kruskal Wallis test with the post hoc Nemenyi test. (C) Percentage of endodermal cells in each radial position suberized close to the hypocotyl junction. Data is binned in 2% of the total root length. Stars indicate the significant difference between each individual radial and longitudinal position to the longitudinal position below according to Welch's two-sample t-test. Scale bar represents 100 µm. (D) Proportion of endodermal cells with expression of *PHO1-H3* in each radial position of the upper 50% of the root. P values of WT and *myb68-2-4* comparisons in each longitudinal position according to unpaired Wilcoxon test are listed.

Figure S2 Expression pattern of *MYB68* in correlation to suberin pattern (A) Suberin pattern of WT (p*GPAT5*:mcritrine) and two independent lines overexpressing

MYB68 in the old endodermis (p*ELTP*:MYB68). Roots were stained with FY as previously described (Naseer, et al., 2012). Zones are shown in percentage of individual root length. Letters indicate significant different groups according to to Kruskal Wallis test with post hoc Nemenyi test. (B) Passage cell occurrence in the fully suberized zone of WT (p*GPAT5*:mcritrine) and two independent lines overexpressing *MYB68* in the old endodermis (p*ELTP*:MYB68). Stars indicate significance according to unpaired Wilcoxon test. (C) *MYB68* Expression onset of *MYB68* in the meristematic region measured by a reporter based on the entire intergenic region of *MYB68* driving expression of a nuclear localized 3x GFP fusion. Measurements were taken of the same roots as in D.Individual letters show significance according to Kruskal Wallis test with post hoc Nemenyi test for T3-7-1 line and according to Anova with post hoc Tukey´s HSD test for T3-8-2 line. (D) Expression start of *MYB68* in each radial position in cells after initials of the two independent alleles. Data points from Figure 3B according to the two independent alleles from p*MYB68*:NSL3xVenus are shown. Individual letters show significance according to the Kruskal Wallis test with post hoc Nemenyi test for T3-7-1 line and according to Anova with post hoc Tukey´s HSD test for T3-8-2 line. (E) *MYB68* expression starts along a cytokinin gradient (6-Benzylaminopurine). Data points from Figure 3C for individual lines without normalization. Star indicated significant difference to WT according to unpaired Wilcoxon test. (F,G) *MYB68* expression start after initials for all endodermal position. Measurements of the same roots in distant to CEID (F) or number of cells to CEID (G). Same data as displayed in Figure 3D, here including the NPAE position. (G) Length of patchy zone of WT and *myb68-2-4* with increasing root age. The same data set from Figure 3F used here for linear regression of data points below 20 mm root length separate from data points above 20 mm root length. The corresponding statistics are in Table S1. XPAE; Xylem pole associated endodermal cells, PPAE; Phloem pole associated endodermal cells, NPAE; non-pole-associated endodermal cells.

Figure S3 Radial distribution of endodermal HKT1 expression (A) Quantification of transcriptional activity of *pHKT1*:NLS-3xmScarlet marker line in WT and *myb68* in the upper 50 % of the root in each radial position. Significance of pairwise comparison was assessed employing Students T test. XPAE; Xylem pole associated endodermal cells, PPAE; Phloem pole associated endodermal cells, NPAE; non-pole-associated endodermal cells.

Table S1: Linear regression analysis of *MYB68* expression start along a time course

Table S2: Linear regression analysis of individual suberin zones against root length along a time course

Table S3: List of DEGs up in *myb68-2-4* vs WT

Table S4: List of DEG up in *myb68-2-4* vs. WT and ns in *myb68 2 4* vs. WT

Table S5: Expression of genes from Table S4 in pELTP:MYB68-4-4 vs WT

Table S6: Expression of known potassium and sodium transporter genes in *myb68-2-4* vs. WT and *myb68-2-4* BAP vs. WT

Table S7: Expression of known gibberellic acid metabolism or signaling genes in *myb68-2-4* vs WT and *myb68-2-4* BAP vs WT

Table S8: Primers use

Materials and methods

Plant growth

In this study Arabidopsis ecotype Columbia-0 was used. Plants were grown, if not otherwise stated for 5-7 days at long day (16h) and 21°C in 140 µmol/m^2/s on half MS (Duchefa) 0.8 % agar (Bacto Agar) 5.8 pH. For cytokinin treatment, seeds were germinated on half MS plates, containing 5,10 or 25 nM N^6 Benzyladenine (CAS #1214-39-7). For abscisic acid (ABA) treatment 5–day old seedlings were transferred to half MS plates containing 1 µM ABA (CAS # 21293-29-8) and grown for 2 days.

Cloning

To generate the transcription reporter lines, the corresponding promoters (ampflied using primer listed in Table S7) were inserted into a modified pUC19 entry vector (Andersen, et al., 2021) via Infusion cloning (Takara) according to the manufacturer description. The coding sequences of the fluorescent protein and the nuclear localization signal or MYB68 were inserted into a pDONR221 entry vector using BP clonase II (Invitrogen) and recombined using LR clonase II (Invitrogen) into the destination vector pED97 containing a FastRed selection (Andersen, et al., 2018). All constructs were transformed into plants using a modified floral dip method (Logemann, et al., 2006) and selected for FastRed (Shimada, et al., 2010) before propagating further. All mutants in MYB genes were described previously (Molina, et al., 2024).

Staining procedures

For overall suberin pattern analysis, seedlings were stained in 0,01 % Flourol Yellow 088 solution (w/v) (interchim) in lactic acid for 30 minutes at 70°C, washed and counterstained in a 0,5% Aniline blue solution (CAS # 66687-07-8) (w/v) in water for 30 minutes at room temperature (Naseer, et al., 2012; LUX, et al., 2005). For radial suberin pattern analysis seedlings were fixed in 4% paraformaldehyde (PFA) (CAS # 30525-89-4), cleared with clearsee (10% xylitol (w/v) (Roth CAS 87-99-0), 15% sodium deoxycholate (w/v) (Thermo scientific CAS # 302-95-4) and 25% urea (w/v) (Roth CAS # 57-13-6)) and stained with 0.01% Fluorol Yellow dissolved in Ethanol as described previously (Sexauer, et al., 2021). For Casparian strip integrity analysis seedlings were incubated in a 10 µg/ml propidium iodide (Sigma Aldrich CAS #25535-16-4) dissolved in water and washed with water before imaging (Naseer, et al., 2012). For analysis of transcriptional reporter lines, cell length and middle cortex quantification, seedlings were fixed, cleared and stained with 0.1 % calcofluor white (Fluorescent Brightener 28 CAS #4404-43-7) dissolved in clearesee (Ursache, et al., 2018).

Transcriptional analysis

For transcriptomic analysis of wild-type and *myb68-2-4* roots, plants were grown in the presence of mock (DMSO) or 25 nM BAP for 6 days under long day conditions. Total RNA from pooled roots was extracted using a Trizol (Invitrogen) adapted ReliaPrep RNA extraction kit (Promega, Z6012) and subjected to quality control, library preparation, and sequencing on the Illumina NovaSeq platform (Novogene) Approximately 25,000,000 reads (150-bp paired-end), on average, were obtained per sample.

Raw reads were processed and cleaned up using fastp (Chen, et al., 2018) with default settings mapped to *A. thaliana* Col-0 genome with the latest annotation (Cheng, et al., 2017) using HISAT2 (Kim, et al., 2019) with default parameters for paired-end reads. Reads per gene without consideration of splicing variants were counted by featureCounts (Liao, et al., 2013) with default parameters. Subsequent statistical analyses were performed using R software (https://www.r-project.org/) unless described otherwise. Differential expression analysis was performed using the *edgeR* package (Robinson, et al., 2009). Library size was normalized by the weighted trimmed mean of M-values (TMM) method, and normalized read counts were fitted to a generalized linear model (GLM) with a negative binomial distribution to identify

significantly differentially expressed genes (DEGs). GO enrichment analysis was performed by Metascape (Zhou, et al., 2019).

Fluorescent in situ hybridization

In situ hybridization chain reaction was performed according to (Oliva, et al., 2022). In short, 6-day old roots were fixed with formaldehyde (CAS # 50-00-0) and dehydrated with a series of increasing concentration of ethanol and incubation at 100% methanol at -20°C overnight. After rehydration with a decreasing series of methanol concentration, cell wall was digested in a solution containing cellulase, pectolyase, macerozyme and pectinase at room temperature for 15 minutes. After proteinase K incubation and additional fixation steps, probe hybridization (*HAK5* probe LOT # RTI354, Molecular Instruments) was performed overnight at 37°C. After washing, 10 µl of 3 µM of B3h1 (LOT#S073325, Molecular Instruments) and H2 (LOT#S075725, Molecular Instruments) hairpin solution was added in amplification buffer, allowing amplification at room temperature for 16 h. As negative controls either a probe specific for the Bacillus subtilis dapB gene (LOT # RTB 421, Molecular Instruments) with the corresponding amplifier B1h1 (LOT #S046325, Molecular Instruments) and B1h2 (LOT #S050925, Molecular Instruments) or just the amplifier used for *HAK5* B3h1 (LOT#S073325, Molecular Instruments) and B3h2 (LOT#S075725, Molecular Instruments) without a probe were used. Excess hairpin was washed away, seedlings were cleared with clearsee (10% xylitol (w/v) (Roth CAS 87-99-0), 15% sodium deoxycholate (w/v) (Thermo scientific CAS 302-95-4) and 25% urea (w/v) (Roth CAS # 57-13-6) and stained with calcofluor white (Fluprescent Brightener 28 CAS #4404-43-7).

Microscopy/imaging

Overall suberin pattern was imaged with AxioZoom 1 Aura and suberin radial pattern, middle cortex, transcriptional marker lines and FISH samples were imaged with confocal laser scanning microscope CLSM Zeiss LSM 980 with the following settings: flourol yellow (ex: 488 nm, em: 500-550 nm), propidium iodide (ex: 561 nm, em: 600-650 nm), calcofluor white (ex: 405 nm, em: 407-466 nm),Venus transcriptional marker line (ex: 514 nm, em: 500-560m), Scarlett signal (ex: 561 nm, em: 570-640 nm), FISH samples (ex: 639 nm, em: 650-680nm). Confocal images were taken with the 40x lense and Zen Connect was used to determine the exact position of image in the root.

Statistics

Statistical analysis was performed in R. Data sets were analyzed for normal distribution using the Shapiro-Wilk test. In case data was normally distributed One-way Anova with post hoc Tukey´s HSD test was performed for multiple comparisons and Students T test or Welch two sample test was performed for comparison of two groups. In case data was not normally distributed for multiple comparison Kruskal Wallis test with post hoc Nemenyi test was used and for comparison of two groups unpaired Wilcoxon test was employed. For time-course experiments linear regression analysis was conducted. All analysis were performed at least twice in independent experiments.

Acknowledgments

All authors thank Ton Timmers and the Central Microscopy facility (CeMic) for microscopy aid. Aristeidis Stamatakis and his greenhouse team at MPIPZ are thanked for help with plant growth. We further thank Niko Geldner for helpful comments on the manuscript.

Funding Research in the lab of TGA is supported by the Sofja Kovalevskaja programme from the Alexander von Humboldt foundation and an independent group leader grant from the Max Planck Society. Research in the lab of LR is supported by the Deutsche Forschungsgemeinschaft (DFG) (Grants: RA2590/4-1 and SFB1101 project B10).

Author contributions

Conceptualization: TGA, LK and LR. Methodology: LK, RTN, DM, LR and TGA. Investigation:LK, RTN and TGA. Visualization: LK, TGA. Funding acquisition: TGA, LR. Main writing: TGA and LK. All authors read and commented on the final version of the manuscript.

Competing interests: All authors declare that they have no competing interests.

Data and materials availability: RNA-seq raw reads and amplicon sequencing raw reads generated in this study have been deposited at National Center for Biotechnology Information under

References

Alassimone, J., Naseer, S., and Geldner, N. (2010). A developmental framework for endodermal differentiation and polarity. Proceedings of the National Academy of Sciences 107, 5214-5219.
Andersen, T.G., Barberon, M., and Geldner, N. (2015). Suberization - the second life of an endodermal cell. Curr Opin Plant Biol 28, 9-15.
Andersen, T.G., Molina, D., Kilian, J., Franke, R.B., Ragni, L., and Geldner, N. (2021). Tissue-autonomous phenylpropanoid production is essential for establishment of root barriers. Current Biology 31, 965-977. e5.
Andersen, T.G., Naseer, S., Ursache, R., Wybouw, B., Smet, W., De Rybel, B., Vermeer, J.E.M., and Geldner, N. (2018). Diffusible repression of cytokinin signalling produces endodermal symmetry and passage cells. Nature 555, 529-533.
Baek, D., Jiang, J., Chung, J.-S., Wang, B., Chen, J., Xin, Z., and Shi, H. (2010). Regulated AtHKT1 Gene Expression by a Distal Enhancer Element and DNA Methylation in the Promoter Plays an Important Role in Salt Tolerance. Plant and Cell Physiology 52, 149-161.
Barberon, M., Vermeer, J.E., De Bellis, D., Wang, P., Naseer, S., Andersen, T.G., Humbel, B.M., Nawrath, C., Takano, J., Salt, D.E., et al. (2016). Adaptation of Root Function by Nutrient-Induced Plasticity of Endodermal Differentiation. Cell 164, 447-59.
Baum, S.F., Dubrovsky, J.G., and Rost, T.L. (2002). Apical organization and maturation of the cortex and vascular cylinder inArabidopsis thaliana (Brassicaceae) roots. American Journal of Botany 89, 908-920.
Berthomieu, P., Conéjéro, G., Nublat, A., Brackenbury, W.J., Lambert, C., Savio, C., Uozumi, N., Oiki, S., Yamada, K., Cellier, F., et al. (2003). Functional analysis of AtHKT1 in Arabidopsis shows that Na(+) recirculation by the phloem is crucial for salt tolerance. Embo j 22, 2004-14.
Binenbaum, J., Wulff, N., Camut, L., Kiradjiev, K., Anfang, M., Tal, I., Vasuki, H., Zhang, Y., Sakvarelidze-Achard, L., Davière, J.-M., et al. (2023). Gibberellin and abscisic acid transporters facilitate endodermal suberin formation in Arabidopsis. Nature Plants 9, 785-802.
Caspary, M.R. (1865). Remarks on the protective sheath and on the formation of the stem of the root. Annals and Magazine of Natural History 16, 382-383.
Chen, S., Zhou, Y., Chen, Y., and Gu, J. (2018). fastp: an ultra-fast all-in-one FASTQ preprocessor. Bioinformatics 34, i884-i890.
Cheng, C.Y., Krishnakumar, V., Chan, A.P., Thibaud-Nissen, F., Schobel, S., and Town, C.D. (2017). Araport11: a complete reannotation of the Arabidopsis thaliana reference genome. Plant J 89, 789-804.
Cui, H. (2015). Cortex proliferation in the root is a protective mechanism against abiotic stress. Plant Signaling & Behavior 10, e1011949.
Cui, H., Kong, D., Wei, P., Hao, Y., Torii, K.U., Lee, J.S., and Li, J. (2014). SPINDLY, ERECTA, and Its Ligand STOMAGEN Have a Role in Redox-Mediated Cortex Proliferation in the Arabidopsis Root. Molecular Plant 7, 1727-1739.
DAVENPORT, R.J., MUÑOZ-MAYOR, A., JHA, D., ESSAH, P.A., RUS, A., and TESTER, M. (2007). The Na+ transporter AtHKT1;1 controls retrieval of Na+ from the xylem in Arabidopsis. Plant, Cell & Environment 30, 497-507.
De Rybel, B., Mähönen, A.P., Helariutta, Y., and Weijers, D. (2016). Plant vascular development: from early specification to differentiation. Nature Reviews Molecular Cell Biology 17, 30-40.
Doblas, V.G., Smakowska-Luzan, E., Fujita, S., Alassimone, J., Barberon, M., Madalinski, M., Belkhadir, Y., and Geldner, N. (2017). Root diffusion barrier control by a vasculature-derived peptide binding to the SGN3 receptor. Science 355, 280-284.
Dolan, L., Janmaat, K., Willemsen, V., Linstead, P., Poethig, S., Roberts, K., and Scheres, B. (1993). Cellular organisation of the Arabidopsis thaliana root. Development 119, 71-84.
Franke, R., Briesen, I., Wojciechowski, T., Faust, A., Yephremov, A., Nawrath, C., and Schreiber, L. (2005). Apoplastic polyesters in Arabidopsis surface tissues – A typical suberin and a particular cutin. Phytochemistry 66, 2643-2658.
Gaymard, F., Pilot, G., Lacombe, B., Bouchez, D., Bruneau, D., Boucherez, J., Michaux-Ferrière, N., Thibaud, J.B., and Sentenac, H. (1998). Identification and disruption of a plant shaker-like outward channel involved in K+ release into the xylem sap. Cell 94, 647-55.
Geldner, N. (2013). The Endodermis. Annual Review of Plant Biology 64, 531-558.

Gierth, M., Mäser, P., and Schroeder, J.I. (2005). The potassium transporter AtHAK5 functions in K(+) deprivation-induced high-affinity K(+) uptake and AKT1 K(+) channel contribution to K(+) uptake kinetics in Arabidopsis roots. Plant Physiol 137, 1105-14.
Hamburger, D., Rezzonico, E., MacDonald-Comber Petétot, J., Somerville, C., and Poirier, Y. (2002). Identification and characterization of the Arabidopsis PHO1 gene involved in phosphate loading to the xylem. Plant Cell 14, 889-902.
Holbein, J., Shen, D., and Andersen, T.G. (2021). The endodermal passage cell – just another brick in the wall? New Phytologist 230, 1321-1328.
Kamiya, T., Borghi, M., Wang, P., Danku, J.M.C., Kalmbach, L., Hosmani, P.S., Naseer, S., Fujiwara, T., Geldner, N., and Salt, D.E. (2015). The MYB36 transcription factor orchestrates Casparian strip formation. Proceedings of the National Academy of Sciences 112, 10533-10538.
Kim, D., Paggi, J.M., Park, C., Bennett, C., and Salzberg, S.L. (2019). Graph-based genome alignment and genotyping with HISAT2 and HISAT-genotype. Nature Biotechnology 37, 907-915.
Kosma, D.K., Murmu, J., Razeq, F.M., Santos, P., Bourgault, R., Molina, I., and Rowland, O. (2014). AtMYB41 activates ectopic suberin synthesis and assembly in multiple plant species and cell types. The Plant Journal 80, 216-229.
Kroemer, K.H.E. Wurzelhaut, Hypodermis und Endodermis der Angiospermenwurzel. In.
Liao, Y., Smyth, G.K., and Shi, W. (2013). featureCounts: an efficient general purpose program for assigning sequence reads to genomic features. Bioinformatics 30, 923-930.
Liberman, L.M., Sparks, E.E., Moreno-Risueno, M.A., Petricka, J.J., and Benfey, P.N. (2015). MYB36 regulates the transition from proliferation to differentiation in the Arabidopsis root. Proceedings of the National Academy of Sciences 112, 12099-12104.
Lin, Y.F., Liang, H.M., Yang, S.Y., Boch, A., Clemens, S., Chen, C.C., Wu, J.F., Huang, J.L., and Yeh, K.C. (2009). Arabidopsis IRT3 is a zinc-regulated and plasma membrane localized zinc/iron transporter. New Phytol 182, 392-404.
Logemann, E., Birkenbihl, R.P., Ülker, B., and Somssich, I.E. (2006). An improved method for preparing Agrobacterium cells that simplifies the Arabidopsis transformation protocol. Plant Methods 2, 16.
LUX, A., MORITA, S., ABE, J., and ITO, K. (2005). An Improved Method for Clearing and Staining Free-hand Sections and Whole-mount Samples*. Annals of Botany 96, 989-996.
Mähönen, A.P., Bishopp, A., Higuchi, M., Nieminen, K.M., Kinoshita, K., Törmäkangas, K., Ikeda, Y., Oka, A., Kakimoto, T., and Helariutta, Y. (2006). Cytokinin signaling and its inhibitor AHP6 regulate cell fate during vascular development. Science 311, 94-8.
Mäser, P., Eckelman, B., Vaidyanathan, R., Horie, T., Fairbairn, D.J., Kubo, M., Yamagami, M., Yamaguchi, K., Nishimura, M., Uozumi, N., et al. (2002). Altered shoot/root Na+ distribution and bifurcating salt sensitivity in Arabidopsis by genetic disruption of the Na+ transporter AtHKT1. FEBS Lett 531, 157-61.
Molina, D., Horvath, S., Zhang, X., Xiao, W., Ragab, N., Ripper, D., Kilian, J., Andersen, T.G., and Ragni, L. (2024). MYB68 orchestrates cork differentiation by regulating stem cell proliferation and suberin deposition. bioRxiv, 2024.03.06.583666.
Naseer, S., Lee, Y., Lapierre, C., Franke, R., Nawrath, C., and Geldner, N. (2012). Casparian strip diffusion barrier in Arabidopsis is made of a lignin polymer without suberin. Proceedings of the National Academy of Sciences 109, 10101-10106.
Nawaz, I., Iqbal, M., Hakvoort, H.W.J., de Boer, A.H., and Schat, H. (2019). Analysis of Arabidopsis thaliana HKT1 and Eutrema salsugineum/botschantzevii HKT1;2 Promoters in Response to Salt Stress in Athkt1:1 Mutant. Mol Biotechnol 61, 442-450.
Oliva, M., Stuart, T., Tang, D., Pflueger, J., Poppe, D., Jabbari, J.S., Gigante, S., Dragwidge, J.M., Whelan, J., Lewsey, M.G., et al. (2022). An environmentally responsive transcriptional state modulates cell identities during root development. bioRxiv, 2022.03.04.483008.
Osakabe, Y., Arinaga, N., Umezawa, T., Katsura, S., Nagamachi, K., Tanaka, H., Ohiraki, H., Yamada, K., Seo, S.-U., Abo, M., et al. (2013). Osmotic Stress Responses and Plant Growth Controlled by Potassium Transporters in Arabidopsis The Plant Cell 25, 609-624.
Paquette, A.J., and Benfey, P.N. (2005). Maturation of the ground tissue of the root is regulated by gibberellin and SCARECROW and requires SHORT-ROOT. Plant Physiol 138, 636-40.

Peterson, C.A., and Enstone, D.E. (1996). Functions of passage cells in the endodermis and exodermis of roots. Physiologia Plantarum 97, 592-598.
Priestley, J., and North, E.E. (1922). Physiological studies in plant anatomy III. The structure of the endodermis in relation to its function. New Phytologist 21, 113-139.
Robinson, M.D., McCarthy, D.J., and Smyth, G.K. (2009). edgeR: a Bioconductor package for differential expression analysis of digital gene expression data. Bioinformatics 26, 139-140.
Scheres, B., Wolkenfelt, H., Willemsen, V., Terlouw, M., Lawson, E., Dean, C., and Weisbeek, P. (1994). Embryonic origin of the Arabidopsis primary root and root meristem initials. Development 120, 2475-2487.
Serra, O., Mähönen, A.P., Hetherington, A.J., and Ragni, L. (2022). The Making of Plant Armor: The Periderm. Annual Review of Plant Biology 73, 405-432.
Sexauer, M., Shen, D., Schön, M., Andersen, T.G., and Markmann, K. (2021). Visualizing polymeric components that define distinct root barriers across plant lineages. Development 148.
Shimada, T.L., Shimada, T., and Hara-Nishimura, I. (2010). A rapid and non-destructive screenable marker, FAST, for identifying transformed seeds of Arabidopsis thaliana. Plant J 61, 519-28.
Shukla, V., Han, J.-P., Cléard, F., Lefebvre-Legendre, L., Gully, K., Flis, P., Berhin, A., Andersen, T.G., Salt, D.E., Nawrath, C., et al. (2021). Suberin plasticity to developmental and exogenous cues is regulated by a set of MYB transcription factors. Proceedings of the National Academy of Sciences 118, e2101730118.
Sitte, P. (1959). Mischkörperdoppelbrechung der Kork-Zellwände. Naturwissenschaften 46, 260-261.
Sunarpi, Horie, T., Motoda, J., Kubo, M., Yang, H., Yoda, K., Horie, R., Chan, W.Y., Leung, H.Y., Hattori, K., et al. (2005). Enhanced salt tolerance mediated by AtHKT1 transporter-induced Na unloading from xylem vessels to xylem parenchyma cells. Plant J 44, 928-38.
Ursache, R., Andersen, T.G., Marhavý, P., and Geldner, N. (2018). A protocol for combining fluorescent proteins with histological stains for diverse cell wall components. Plant J 93, 399-412.
Wunderling, A., Ripper, D., Barra-Jimenez, A., Mahn, S., Sajak, K., Targem, M.B., and Ragni, L. (2018). A molecular framework to study periderm formation in Arabidopsis. New Phytol 219, 216-229.
Xu, X., Guerriero, G., Domergue, F., Beine-Golovchuk, O., Cocco, E., Berni, R., Sergeant, K., Hausman, J.-F., and Legay, S. (2023). Characterization of MdMYB68, a suberin master regulator in russeted apples. Frontiers in Plant Science 14.
Yoshida, H., Hirano, K., Sato, T., Mitsuda, N., Nomoto, M., Maeo, K., Koketsu, E., Mitani, R., Kawamura, M., Ishiguro, S., et al. (2014). DELLA protein functions as a transcriptional activator through the DNA binding of the indeterminate domain family proteins. Proc Natl Acad Sci U S A 111, 7861-6.
Zhang, Z.-L., Ogawa, M., Fleet, C.M., Zentella, R., Hu, J., Heo, J.-O., Lim, J., Kamiya, Y., Yamaguchi, S., and Sun, T.-p. (2011). SCARECROW-LIKE 3 promotes gibberellin signaling by antagonizing master growth repressor DELLA in Arabidopsis. Proceedings of the National Academy of Sciences 108, 2160-2165.
Zhou, Y., Zhou, B., Pache, L., Chang, M., Khodabakhshi, A.H., Tanaseichuk, O., Benner, C., and Chanda, S.K. (2019). Metascape provides a biologist-oriented resource for the analysis of systems-level datasets. Nature Communications 10, 1523.

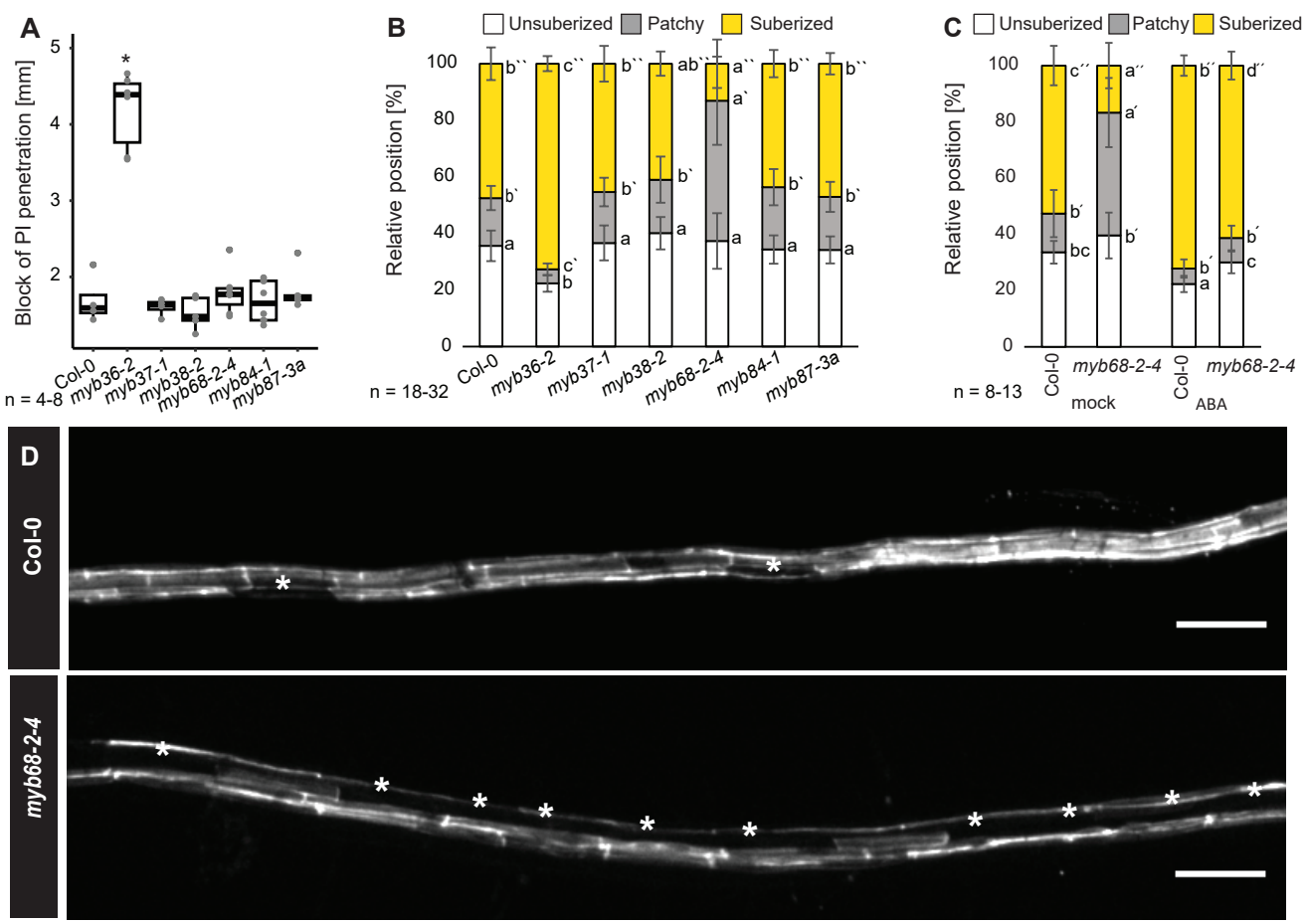

Figure 1 | Formation of endodermal barriers in MYB36-like mutants

A) Quantification of Casparian strip function by measuring the absolute distance from the root tip to the onset of PI penetration blockage into the vasculature (Naseer, et al., 2012). B), C) Suberization patterning in roots stained with the dye Fluorol yellow 088 (FY) (Naseer, et al., 2012). D) Images depict part of the suberized zone of FY (LUX, et al., 2005) roots. Individual letters depict significance (P<0.05) according to a Kruskal Wallis test with a post hoc Nemenyi test. Scale bar represents 100 µm. In A, asterisks depict significant difference to WT according to unpaired Wilcoxon test, whereas in D, asterisks mark individual passage cells. ABA; Abscic acid

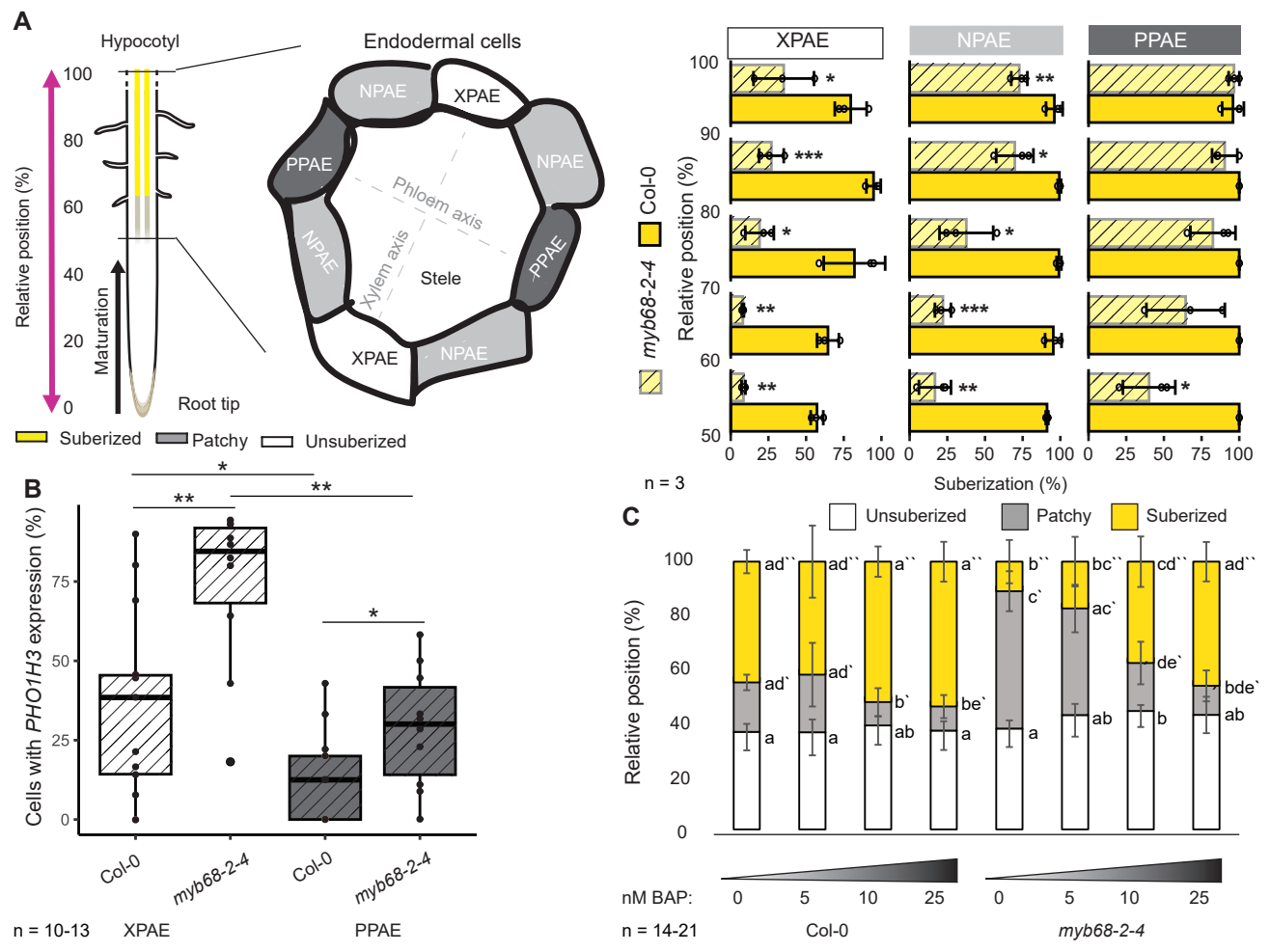

Figure 2 | Analysis of suberin patterning and passage cell occurence

LA) Analysis of radial suberin patterning along the upper 50% of the root. Roots were fixed and stained with Fluorol Yellow 088 (FY) (LUX, et al., 2005) and the proportion of suberized cells were quantified and binned in longitudinal sections. Asterisks indicate significant difference between Col-0 and myb68-2-4 in each longitudinal position according to students Welch two sample t test (* p value < 0.05, ** p value < 0.005, *** p < 0.0005). B) Proportion of endodermal cells with expression of PHO1H3 in XPAE vs PPAE of the upper 50% of the root (similar sections as in A). Stars indicate significant difference between WT and myb68-2-4 in each longitudinal position according to unpaired Wilcoxon test (* p value < 0.05). C) Suberization pattern in roots grown in presence of increasing amounts of the artificial cytokinin 6 Benzyl-aminopurine (BAP). Individual letters depict significance (P<0.05) according to a Kruskal Wallis test with a post hoc Nemenyi test. XPAE; Xylem pole associated endodermis, PPAE; Phloem pole associated endodermis, NPAE; Non-pole associated endodermis.

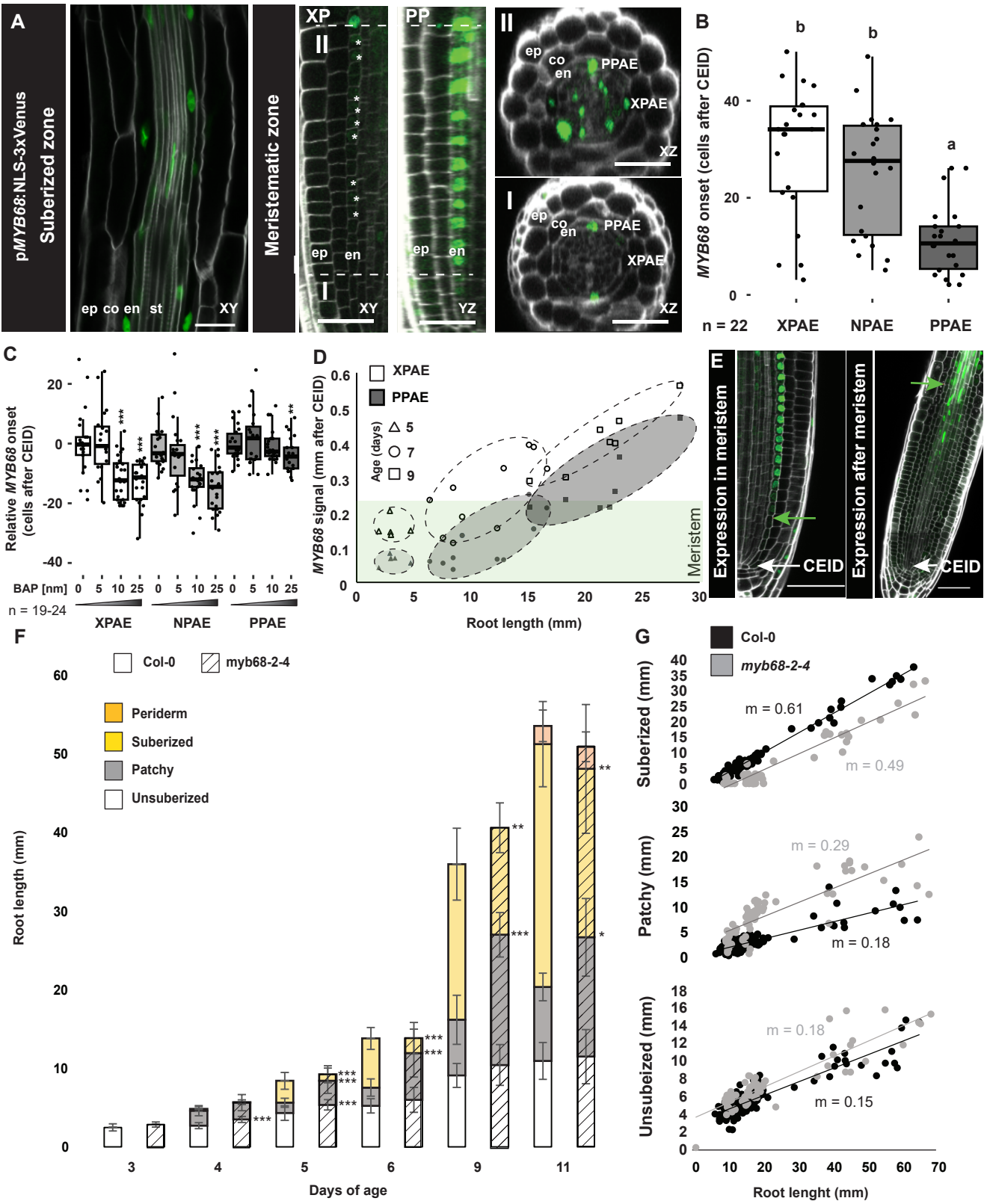

Figure 3 | Analysis of MYB68 expression and age-dependent suberin patterning

A) Activity of MYB68 in roots of 6-day-old seedlings expressing a transcriptional reporter for MYB68 activity (pMYB68:NLS3xVenus). Roots were fixed in Clearsee and cell walls were stained using calcofluor white (Ursache, et al., 2018) Scale bar represents 50 µm. The two dashed lines mark the position of cross sections I and II. B) Analysis of expression onset of MYB68 in the meristematic zone of plants from A. Individual letters show significance according to Kruskal Wallis test with post hoc Nemenyi test. C) Changes of MYB68 expression onset in roots germinated in the presence of increasing amounts of the artificial cytokinin 6 Benzyl-aminopurine (BAP). Onset is normalized to the average of nontreated roots in each radial position. Asterisks indicate significant differences compared to the untreated sample in each radial position according to unpaired Wilcoxon text (* p value < 0.05, ** p < 0.001, *** p < 0.0001). D) Expression onset in the endodermis of MYB68 measured along a time course (Linear regression statistics can be found in Table S1). E) Images depicting MYB68 expression start within the meristem 5- and 9-day-old roots expressing a MYB68 transcriptional reporter similar as A. Arrows marks the cortex/endodermal initial daughter cell (CEID). Scale bar represents 50 µm. F) Time-course analysis of suberin patterning in 3-11 day-old roots stained with fluorol yellow 088 (LUX, et al., 2005). Asterisks indicate significant differences between Col-0 and myb68-2-4 at each time point, and in each zone via an unpaired Wilcoxon text (* p value < 0.05, ** p value < 0.005, *** p value < 0.0005). G) Relation of suberization zone length to root length of individual roots in 5-11-day old roots. Values for the slopes are displayed (m). Corresponding statistical values can be found in Table S2. XPAE; Xylem pole associated endodermis, PPAE; Phloem pole associated endodermis, NPAE; non-pole associated endodermis. Ep; epidermis, co; Cortex, en; Endodermis, st; Stele. XP; Xylem pole, PP; Phloem pole.

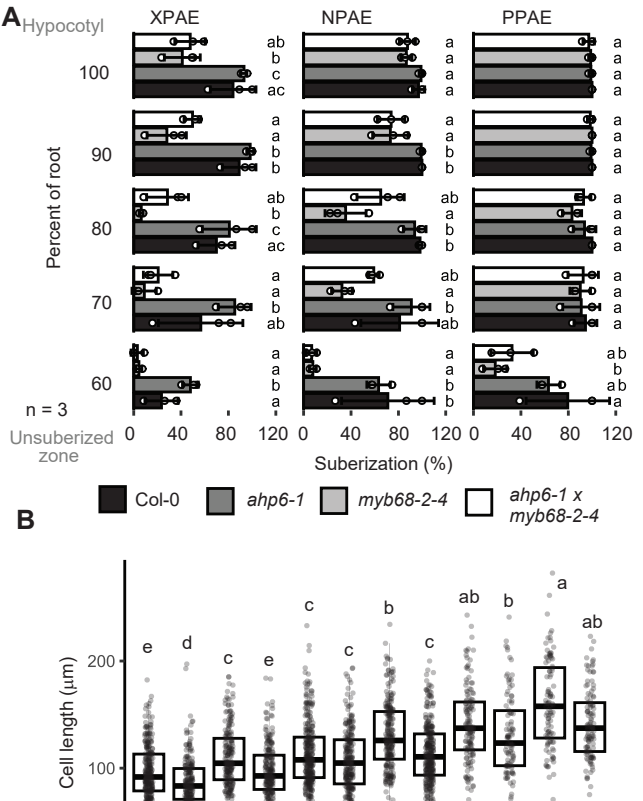

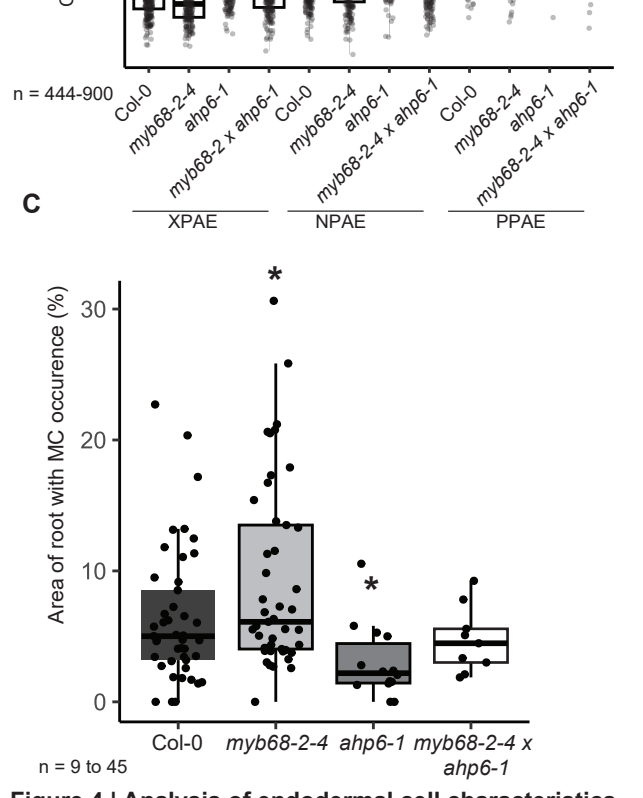

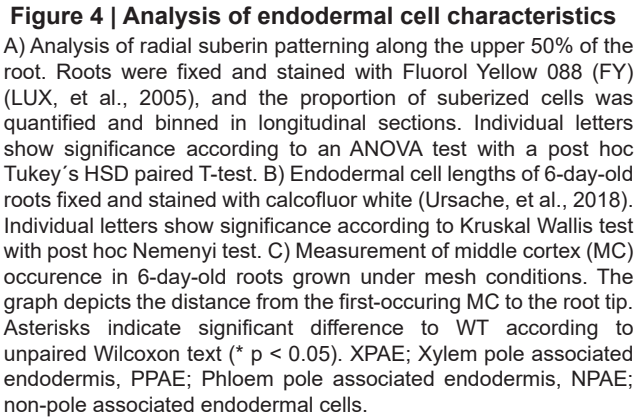

Figure 4 | Analysis of endodermal cell characteristics

A) Analysis of radial suberin patterning along the upper 50% of the root. Roots were fixed and stained with Fluorol Yellow 088 (FY) (LUX, et al., 2005), and the proportion of suberized cells was quantified and binned in longitudinal sections. Individual letters show significance according to an ANOVA test with a post hoc Tukey´s HSD paired T-test. B) Endodermal cell lengths of 6-day-old roots fixed and stained with calcofluor white (Ursache, et al., 2018). Individual letters show significance according to Kruskal Wallis test with post hoc Nemenyi test. C) Measurement of middle cortex (MC) occurence in 6-day-old roots grown under mesh conditions. The graph depicts the distance from the first-occuring MC to the root tip. Asterisks indicate significant difference to WT according to unpaired Wilcoxon text (* $p < 0.05$). XPAE; Xylem pole associated endodermis, PPAE; Phloem pole associated endodermis, NPAE; non-pole associated endodermal cells.

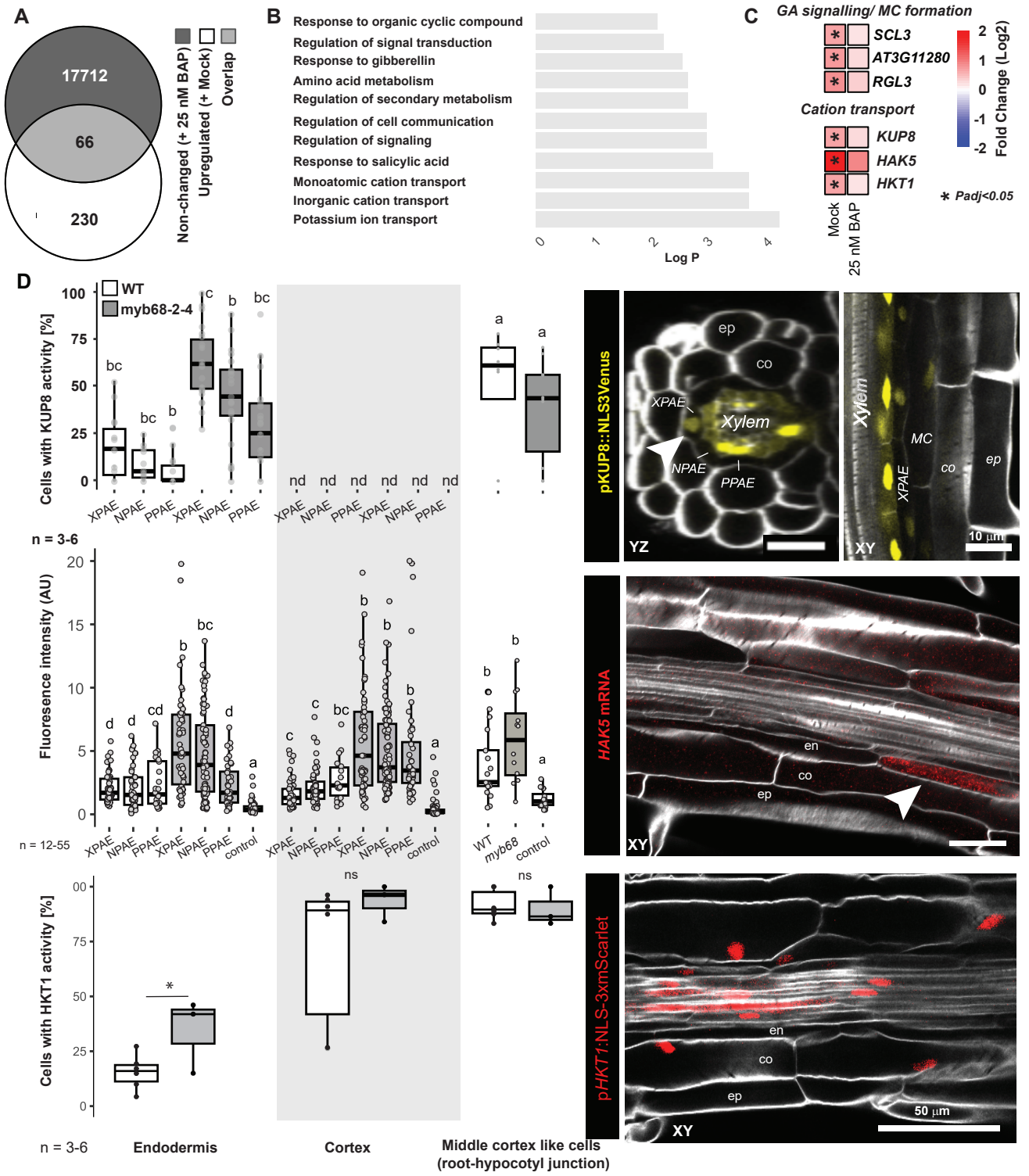

Figure 5 | Passage cell-associated transcriptional analysis

A) Overlap of upregulated genes in 6-day-old Col-0 vs myb68-2-4 roots (padj <0.05) and genes with non-significant changes in WT vs. myb68-2-4 when germinated on BAP (25 nM 6-Benzyl-aminopurine). B) GO-term analysis of the 66 overlapping genes from A (Zhou, et al., 2019)C) Heatmap of selected middle cortex (MC) regulating genes as well as cation transporters in the comparisons from A (all genes can be found in Table S6 and S7). D) Quantification of transcriptional activity of gene expression in the upper 50 % of the root as well as MC-like cells close to the root-hypocotyl junction. Expression analysis of KUP8 and HKT1 in WT and myb68-2-4 was performed using the corresponding transcriptional marker lines (pKUP8:NLS3xVenus, pHKT1:NLS-3xmScarlet). For HAK5 mRNA, fluorescence in situ hybridization was employed. As negative control either a probe specific for the Bacillus subtilis dapB (LOT # RTB 421) with the corresponding amplifier B1h1 (LOT #S046325) and B1h2 (LOT # S050925) or only the amplifier used for HAK5 B3h1 (LOT#S073325) and B3h2 (LOT#S075725) without a probe were used. Individual letters show significance according to Kruskal Wallis test with post hoc Nemenyi test. XPAE; Xylem pole associated endodermal cells, PPAE; Phloem pole associated endodermal cells, NPAE; non-pole-associated endodermal cells. Ep; Epidermis, Co; Cortex, En; Endodermis, nd; not detected, ns; not significant. Scale bars represent 25 µm unless otherwise mentioned.

hyb68-2-4 when germinated on BAP (25 nM 6-Benzyl-aminopurine). B) GO-ter
019)C) Heatmap of selected middle cortex (MC) regulating genes as well as

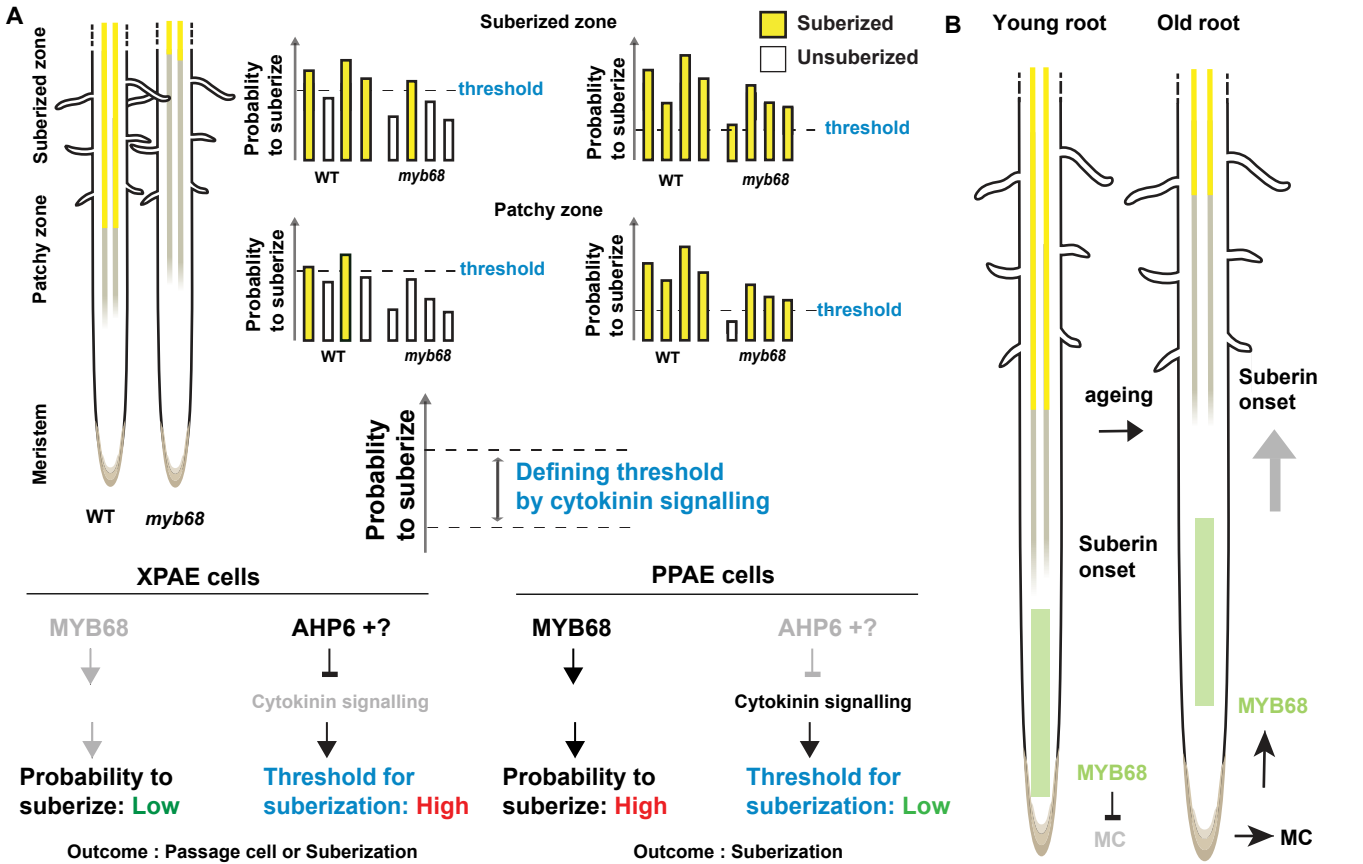

Figure 6 | Model of radial endodermal development

A) Overlap of upregulated genes in 6-day-old Col-0 vs myb68-2-4 roots (padj <0.05) and genes with non-significant changes in WT vs. myb68-2-4 when germinated on BAP (25 nM 6-Benzyl-aminopurine). B) GO-term analysis of the 66 overlapping genes from A (Zhou, et al., 2019)C) Heatmap of selected middle cortex (MC) regulating genes as well as cation transporters in the comparisons from A (all genes can be found in Table S6 and S7). D) Quantification of transcriptional activity of gene expression in the upper 50 % of the root as well as MC-like cells close to the root-hypocotyl junction. Expression analysis of KUP8 and HKT1 in WT and myb68-2-4 was performed using the corresponding transcriptional marker lines (pKUP8:NLS3xVenus, pHKT1:NLS-3xmScarlet). For HAK5 mRNA, fluorescence in situ hybridization was employed. As negative control either a probe specific for the Bacillus subtilis dapB (LOT # RTB 421) with the corresponding amplifier B1h1 (LOT #S046325) and B1h2 (LOT # S050925) or only the amplifier used for HAK5 B3h1 (LOT#S073325) and B3h2 (LOT#S075725) without a probe were used. Individual letters show significance according to Kruskal Wallis test with post hoc Nemenyi test. XPAE; Xylem pole associated endodermal cells, PPAE; Phloem pole associated endodermal cells, NPAE; non-pole-associated endodermal cells. Ep; Epidermis, Co; Cortex, En; Endodermis, nd; not detected, ns; not significant. Scale bars represent 25 µm unless otherwise mentioned.

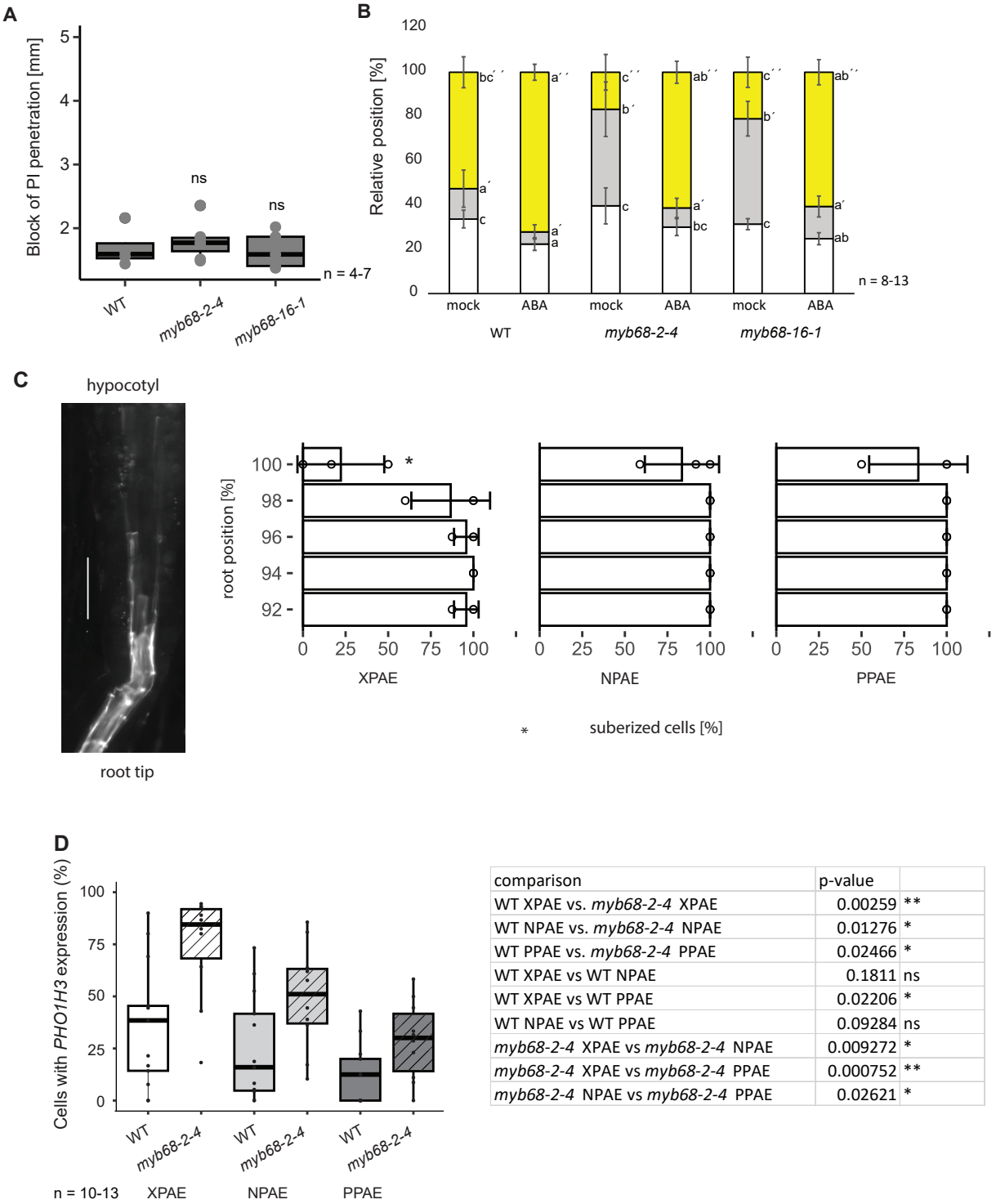

comparison	p-value	
WT XPAE vs. *myb68-2-4* XPAE	0.00259	**
WT NPAE vs. *myb68-2-4* NPAE	0.01276	*
WT PPAE vs. *myb68-2-4* PPAE	0.02466	*
WT XPAE vs WT NPAE	0.1811	ns
WT XPAE vs WT PPAE	0.02206	*
WT NPAE vs WT PPAE	0.09284	ns
myb68-2-4 XPAE vs *myb68-2-4* NPAE	0.009272	*
myb68-2-4 XPAE vs *myb68-2-4* PPAE	0.000752	**
myb68-2-4 NPAE vs *myb68-2-4* PPAE	0.02621	*

Figure s1 | Endodermal barriers

(A) Quantification of Casparian strip integrity by measuring the distance from the root tip to the onset of PI penetration as described before (Naseer, et al., 2012). Star indicated a significant difference to WT according to the unpaired Wilcoxon test. (B) Staining of suberin using the dye Fluorol yellow (FY) (Naseer, et al., 2012), graphs depict the relative proportion of the root which is unsuberized (white), suberized in a patchy pattern (grey), and fully suberized (yellow). Transfer to 1µM ABA or mock 2 days before staining. Individual letters show significance according to the Kruskal Wallis test with the post hoc Nemenyi test. (C) Percentage of endodermal cells in each radial position suberized close to the hypocotyl junction. Data is binned in 2% of the total root length. Stars indicate the significant difference between each individual radial and longitudinal position to the longitudinal position below according to Welch's two-sample t-test. Scale bar represents 100 µm. (D) Proportion of endodermal cells with expression of PHO1-H3 in each radial position of the upper 50% of the root. P values of WT and myb68-2-4 comparisons in each longitudinal position according to unpaired Wilcoxon test are listed.

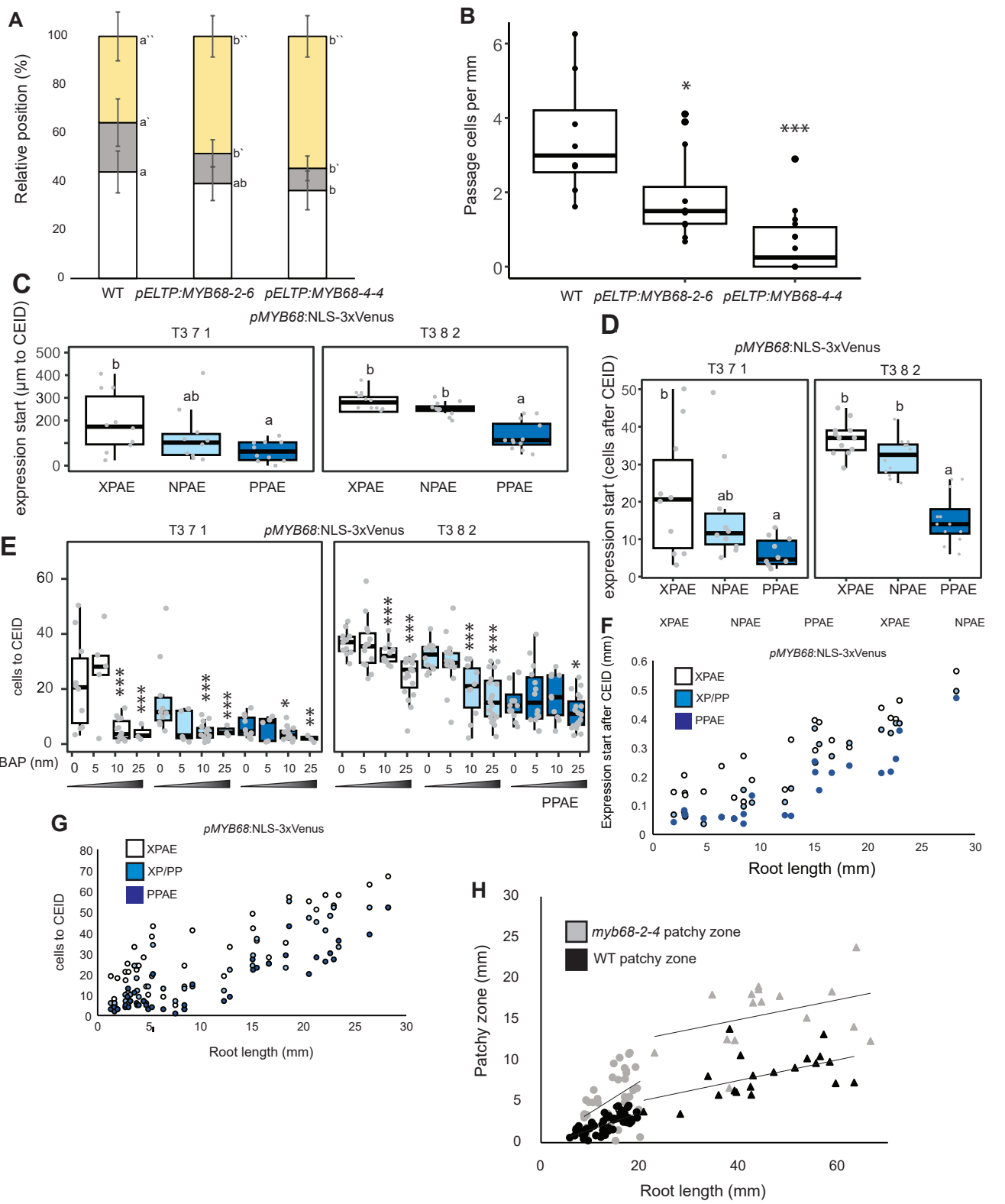

Figure S2 | Expression pattern of MYB68 in correlation to suberin pattern

Suberin pattern of WT (pGPAT5:mcritrine) and two independent lines overexpressing MYB68 in the old endodermis (pELTP:MYB68). Roots were stained with FY as previously described (Naseer, et al., 2012). Zones are shown in percentage of individual root length. Letters indicate significant different groups according to to Kruskal Wallis test with post hoc Nemenyi test. (B) Passage cell occurrence in the fully suberized zone of WT (pGPAT5:mcritrine) and two independent lines overexpressing MYB68 in the old endodermis (pELTP:MYB68). Stars indicate significance according to unpaired Wilcoxon test. (C) MYB68 Expression onset of MYB68 in the meristematic region measured by a reporter based on the entire intergenic region of MYB68 driving expression of a nuclear localized 3x GFP fusion. Measurements were taken of the same roots as in D.Individual letters show significance according to Kruskal Wallis test with post hoc Nemenyi test for T3-7-1 line and according to Anova with post hoc Tukey´s HSD test for T3-8-2 line. (D) Expression start of MYB68 in each radial position in cells after initials of the two independent alleles. Data points from Figure 3B according to the two independent alleles from pMYB68:NSL3xVenus are shown. Individual letters show significance according to the Kruskal Wallis test with post hoc Nemenyi test for T3-7-1 line and according to Anova with post hoc Tukey´s HSD test for T3-8-2 line. (E) MYB68 expression starts along a cytokinin gradient (6-Benzylaminopurine). Data points from Figure 3C for individual lines without normalization. Star indicated significant difference to WT according to unpaired Wilcoxon test. (F,G) MYB68 expression start after initials for all endodermal position. Measurements of the same roots in distant to CEID (F) or number of cells to CEID (G). Same data as displayed in Figure 3D, here including the NPAE position. (G) Length of patchy zone of WT and myb68-2-4 with increasing root age. The same data set from Figure 3F used here for linear regression of data points below 20 mm root length separate from data points above 20 mm root length. The corresponding statistics are in Table S1. XPAE; Xylem pole associated endodermal cells, PPAE; Phloem pole associated endodermal cells, NPAE; non-pole-associated endodermal cells.

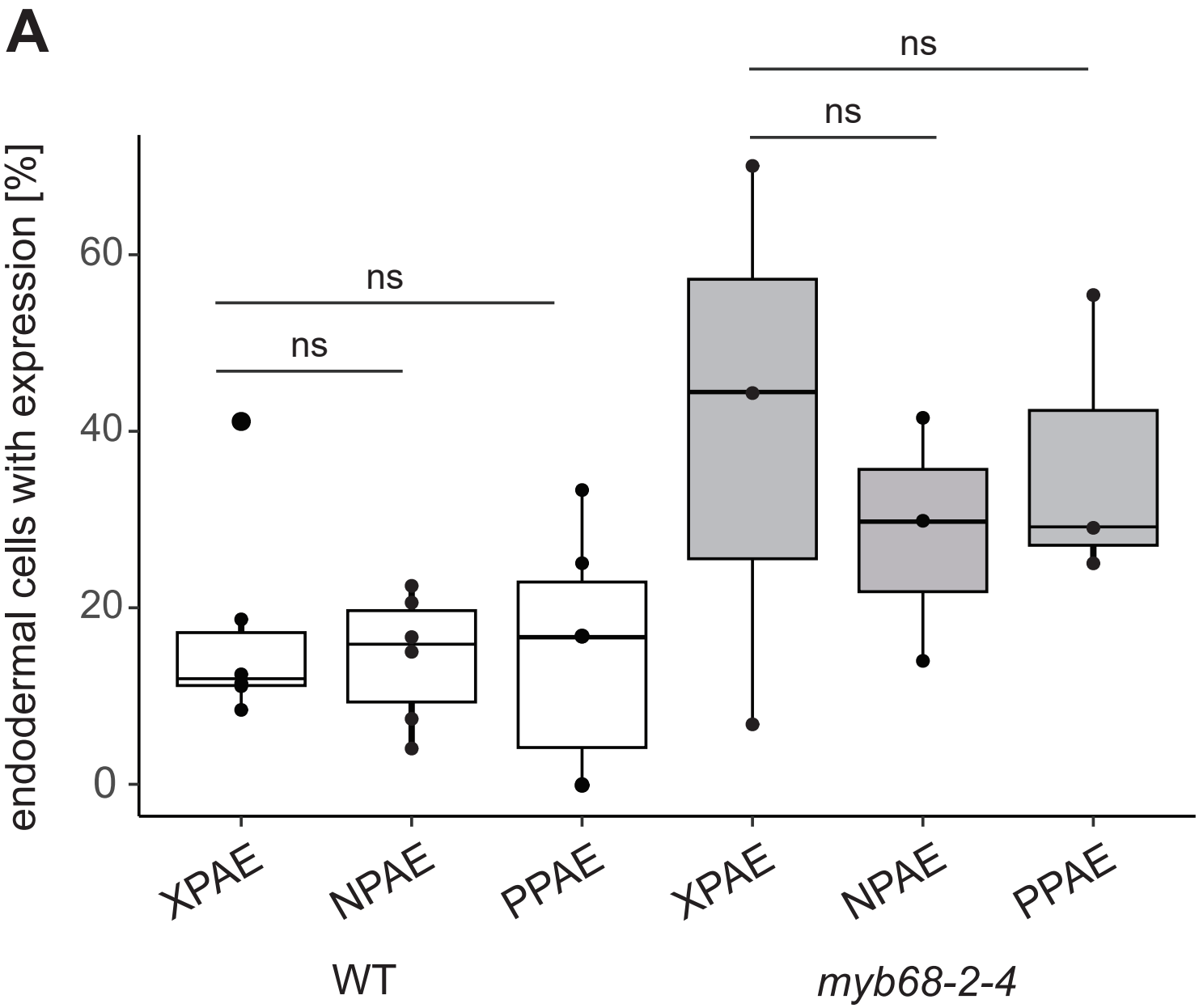

Figure S3 | Radial distribution of endodermal HKT1 expression

(A) Quantification of transcriptional activity of pHKT1:NLS-3xmS-carlet marker line in WT and myb68 in the upper 50 % of the root in each radial position. Significance of pairwise comparison was assessed employing Students T test. XPAE; Xylem pole associated endodermal cells, PPAE; Phloem pole associated endodermal cells, NPAE; non-pole-associated endodermal cells.